High Entropy Alloys & Materials (2023) 1:72–83
https://doi.org/10.1007/s44210-022-00003-7

ORIGINAL PAPER

Grain Size Tailoring to Control Strain Hardening and Improve the Mechanical Properties of a CoCrFeNiMn High-Entropy Alloy

Hamed Shahmir[1] · Mohammad Sajad Mehranpour[2] · Seyed Amir Arsalan Shams[3] · Chong Soo Lee[3] · Terence G. Langdon[4]

Received: 27 April 2022 / Accepted: 19 July 2022 / Published online: 19 August 2022

Abstract

An equiatomic CoCrFeNiMn high-entropy alloy was processed by severe plastic deformation followed by post-deformation annealing over a range of temperatures and times leading to a wide range of grain sizes from ~ 0.05 to ~ 70 μm. The results demonstrate there is a sharp evolution in grain size and hardness after annealing above 800 °C due to coarsening facilitated by the dissolution of precipitates together with a high rate of diffusion at high temperatures. Grain growth behavior revealed an incremental low value grain growth exponent with increasing annealing temperature together with a high value activation energy for grain growth of ~ 440 kJ mol^{-1}. A critical grain size of ~ 2 μm is proposed in which deformation-induced twinning is suppressed during plastic deformation. Nevertheless, slip and deformation-induced twinning are deformation mechanisms occurring in samples with grain sizes above this critical value. A model is presented for engineering the grain size by controlling the annealing parameters in the fine grain size range to benefit from the advantages of deformation-induced twining in the CoCrFeNiMn alloy.

Keywords Deformation-induced twinning · Grain refinement · High-entropy alloy · Microstructure engineering · Thermomechanical treatment

Introduction

One of the first and well-studied high-entropy alloys (HEAs) is the equiatomic CoCrFeNiMn alloy which has a significant potential for use in future industrial applications. This potential arises because of its extraordinary properties such as a high fracture toughness over a wide range of temperatures including cryogenic temperature, a high ductility, a high phase stability and an excellent resistance to hydrogen embrittlement [1–7]. This alloy shows superior ductility (up to 85% at room temperature and lower temperatures) due to its simple *fcc* phase and the activation of dislocation slip and twinning as the most important deformation mechanisms [7]. Basically, the CoCrFeNiMn alloy has a great potential for easy deformation by dislocation slip due to the large number of slip systems [8]. Nevertheless, the relatively low stacking fault energy (SFE) of the alloy, ~ 21 mJ m^{-2} [9–12], affects the deformation mechanism. It is well-established that deformation-induced twinning is a major deformation mechanism in *fcc* metals with SFE lower than ~ 25 mJ m^{-2} and, accordingly, it is expected that deformation-induced twinning will be activated along with dislocation slip as the controlling deformation mechanisms in the CoCrFeNiMn HEA [11, 13–16]. It was shown that deformation-induced twinning increases ductility by changing the strain hardening curve [17, 18]. In addition, it produces hardening due to a build-up of back-stress together with preventing the planar glide of dislocations which consequently can improve the strength and uniform elongation simultaneously. It is important to note that the latter is responsible for facilitating remarkable workability in the alloy.

✉ Hamed Shahmir
shahmir@modares.ac.ir

[1] Department of Materials Engineering, Tarbiat Modares University, Tehran, Iran

[2] School of Metallurgy and Materials, College of Engineering, University of Tehran, Tehran, Iran

[3] Graduate Institute of Ferrous Technology, Pohang University of Science and Technology, Pohang 37673, South Korea

[4] Materials Research Group, Department of Mechanical Engineering, University of Southampton, Southampton SO17 1BJ, UK

Many attempts were conducted to improve the intrinsic low strength of the single *fcc*-phase CoCrFeNiMn HEA without producing any significant sacrifice of ductility [7, 8, 19–26] using grain refinement as one of the most effective procedures for improving strength based on the well-known Hall–Petch strengthening. It is important to note that deformation-induced twinning is responsible for significant grain refinement after imposing a sufficient strain during plastic deformation and this is known as the dynamic Hall–Petch effect which decreases the dislocation mean free path and should thereby increase the strength of the material [18]. The most important and effective procedure for introducing grain refinement is through the use of severe plastic deformation (SPD) followed by short-term annealing to tailor an ultrafine-grained microstructure which will improve the strength with no significant sacrifice of ductility in the CoCrFeNiMn alloy [27–29].

Basically, the grain size plays an active role to activate deformation-induced twinning during plastic deformation. The occurrence of deformation-induced twinning was confirmed in many investigations after deformation of the CoCrFeNiMn HEA alloy with different grain sizes, from several tens to a few micrometers, at both room and cryogenic temperatures [8, 10, 13, 30–32]. However, it was reported earlier that grain refinement, predominantly down to the specific grain size range of ultrafine-grained materials (< 1 μm), may increase the SFE and suppress deformation twinning [33]. It was also shown that there is a critical grain size in which no deformation twinning is observed during plastic deformation such that dislocation slip is the only mechanism accommodating the imposed strain [33–35]. This phenomenon may affect the mechanical aspects of the alloy including the strain hardening behaviour, strength, uniform elongation and workability. The present investigation was, therefore, initiated to provide a systematic demonstration of the role of grain size, especially in the range of a few microns to submicrons fabricated by SPD followed by short-term annealing, on the deformation mechanisms and mechanical properties of the CoCrFeNiMn HEA. The present investigation is focused on the grain growth kinetics to improve the understanding of grain size control during post-deformation annealing of the CoCrFeNiMn HEA. This research is important because the grain size, within the fine and ultrafine grain range, affects the deformation mechanism as an important parameter which determines the mechanical properties.

Materials and Methods

High purity elements of Co, Cr, Fe, Ni, and Mn were used to fabricate an equiatomic HEA by an arc melting method using a water-cooled copper crucible to make the alloy. The arc was formed in a high purity Ar atmosphere using a non-consumable tungsten electrode and the alloy was remelted several times to obtain the best chemical homogeneity. The as-cast alloy was homogenized at 1000 °C for 16 h under an Ar-controlled atmosphere and then disks of 10 mm in diameter and thicknesses of ~ 1 mm were prepared by electro-discharge machining. These disks were polished mechanically to final thicknesses of ~ 0.8 mm. The disks were processed by high-pressure torsion [36] under quasi-constrained conditions in which there is a small outflow of material around the periphery of the disk [37]. The HPT was conducted using an applied pressure of 6.0 GPa and processing through a total of five rotations. After HPT processing the specimens were subjected to annealing at different temperatures and times.

Foils for scanning transmission electron microscopy (STEM) were prepared after the HPT processing using a focused ion beam (FIB) Zeiss Nvision 40 FIB facility at 3 mm from the disk centers in the normal sections of the disks so that the normals of the images lay in the shear direction. The microstructures of the annealed specimens were studied using optical microscopy (OM) and scanning electron microscopy (SEM) after grinding through 800, 1200 and 4000 grit SiC papers, polishing using a 40 nm colloidal silica suspension and then etching with a solution of 50 mL H_2O, 50 mL HCl and 10 g $CuSO_4$. The electron channel contrast imaging (ECCI) technique was also used at a voltage of 15 kV, a probe current of 18 nA and with a working distance of 5 mm in a field emission SEM (FESEM 7900, JEOL, Japan). Grain size measurements were based on the standard intercept method (ASTM E112).

Hardness measurements were taken using a Vickers microhardness tester with a load of 500 gf and dwell times of 10 s where each reported value represents the average of seven separate hardness values. Tensile specimens with gauge dimensions of $1.1 \times 1.0 \times 0.6$ mm^3 were cut from symmetric off-centre positions near the edges of each disk using electro-discharge machining. Tensile tests were conducted on the samples using an initial strain rate of ~ 1.0×10^{-3} s^{-1} with a Zwick universal testing machine in which the tensile strengths were derived directly from the curves and the elongations were estimated by carefully measuring the gauge lengths before and after tensile testing using an optical microscope.

Results

Grain Size and the Grain Growth Behaviour During Post-deformation Annealing

Figure 1 shows the microstructure of the sample after SPD and post-deformation annealing at 800 and 900 °C.

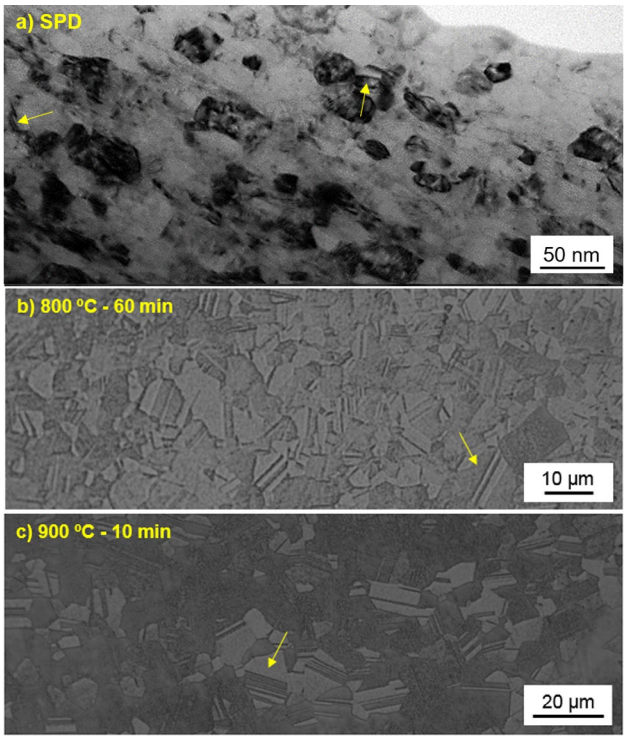

Fig. 1 Microstructure of CoCrFeNiMn HEA after **a** severe plastic deformation by HPT (STEM image), and **b**, **c** after post-deformation annealing (OM images)

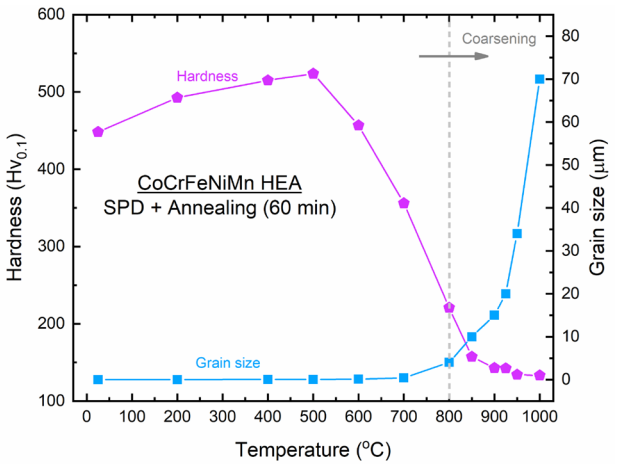

Fig. 2 Hardness and grain size changes of CoCrFeNiMn HEA during post-deformation annealing at different temperatures for 60 min

This set of microstructures reveals nano and fine equiaxed grains in the severely deformed and the annealed samples, respectively, with an absence of any secondary phases. It is important to note also that the microstructure before HPT processing (not shown) was typical of a fully annealed sample consisting of equiaxed grains with an average grain size of ~ 120 µm. Nano-deformation twins and annealing twins are shown by yellow arrows in the severely deformed and annealed samples, respectively. These images clearly reveal the very significant grain refinement after SPD and appropriate heat treatment.

Detailed information is shown in Fig. 2 for the average grain sizes of samples after post-deformation annealing at different temperatures for 60 min together with the microhardness measurements. The results confirm there is no significant change in grain size up to 800 °C but thereafter at temperatures > 800 °C the grain size rapidly increases due to a coarsening effect. The trend of the hardness values shows an increase from 450 Hv (as a deformed condition) to 520 Hv after annealing at 500 °C followed by a rapid decrease with increasing annealing temperatures up to 1000 °C which then reaches a hardness value of ~ 130 Hv as in the initial condition before deformation. The significant grain refinement and the introduction of defects during SPD are responsible for this remarkable increment of hardness by a factor of ~ 3.5. These grain size and hardness changes are due to the formation of precipitates during annealing at < 800 °C and the subsequent dissolution of the precipitates at temperatures > 800 °C. The formation of Cr-rich precipitates at < 800 °C was reported earlier in this HEA [6, 7, 27, 29, 38–41] where the pinning effect of precipitates on the grain boundaries is the main obstacle to a coarsing phenomena at temperatures below ~ 800 °C. However, a dissolution of these precipitates and the associated high rate of diffusion at high temperatures are crucial factors in the occurrence of significant coarsening at temperatures greater than ~ 800 °C.

Based on the scope of this investigation, it was important to focus on the coarsening behavior at higher temperatures. Accordingly, Fig. 3a shows the grain size in terms of different holding times at temperatures of 800, 850, 900 and 950 °C. As expected, the grain size increases with increasing annealing time and this increment is larger at the higher temperatures. To study the grain growth behavior, a parabolic grain growth kinetics was considered in the present work based on Eq. 1 [42–44]:

$$D^n - D_0{}^n = kt \tag{1}$$

where D, D_0, n, k, and t are grain size, initial grain size (~ 0.05 µm), grain growth exponent, a temperature-dependent constant and the time (min), respectively. It is worth noting that D_0 was ignored due to the very small value of D_0 by comparison with D so that Eqs. 2 and 3 can be derived as:

$$D^n = kt \tag{2}$$

and

$$\mathrm{Ln}t = n\mathrm{Ln}D - \mathrm{Ln}k \tag{3}$$

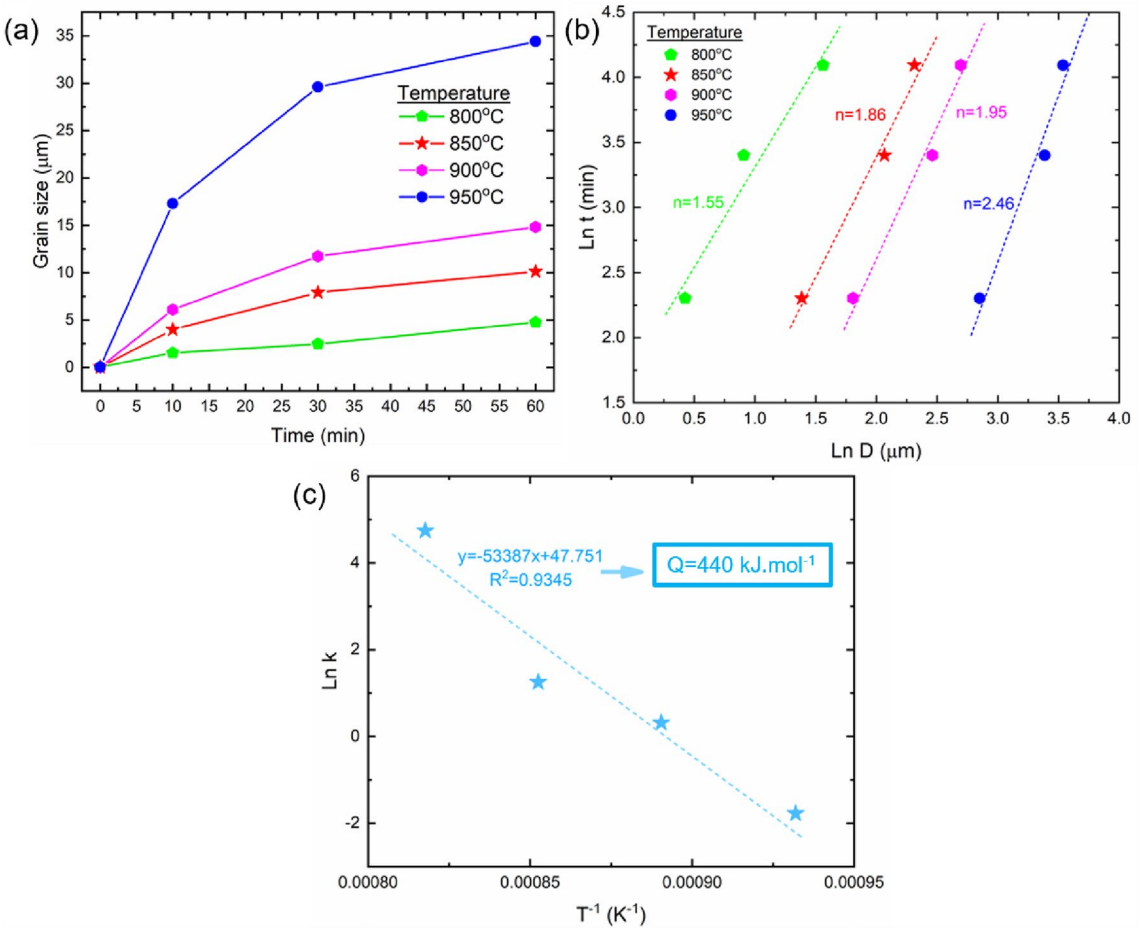

Fig. 3 **a** Effects of annealing temperature and holding time on grain size, **b** Plot of Lnt versus LnD, and **c** Plot of Lnk as a function of T^{-1} used for determining the activation energy for grain growth

A plot of Ln t versus Ln D then yields a straight line for each temperature from which the slope, n, and the intercept, Lnk, can be readily calculated as shown in Fig. 3b. According to these results, the n value increases with increasing temperature. The dependence of k on the grain growth activation energy and temperature is given by the following relationship:

$$k = k_0 \exp\left(-\frac{Q}{RT}\right) \tag{4}$$

where T is the temperature in degrees Kelvin, K_0 is a constant, Q is the grain growth activation energy (kJ mol^{-1}) and R is the gas constant (8.31 J mol^{-1} K^{-1}). Thus,

$$\mathrm{Ln}k = \mathrm{Ln}k_0 - \frac{Q}{RT} \tag{5}$$

According to the above equation and Fig. 3c, the grain growth activation energy, Q, was calculated as ~ 440 kJ mol^{-1}.

Mechanical Properties

Figure 4a represents a set of true stress-true strain diagrams of the single-phase CoCrFeNiMn HEA with different grain sizes in the range of 0.05–120 μm which were obtained after SPD followed by post-deformation annealing. The results show a significant increase in strength of the nano-grain sample after SPD but with a corresponding decrease in the measured elongations to failure. The results demonstrate that the elongations to failure are restored and increase at the expense of a decrease in strength with increasing grain size after annealing. Figure 4b shows a summary of the mechanical

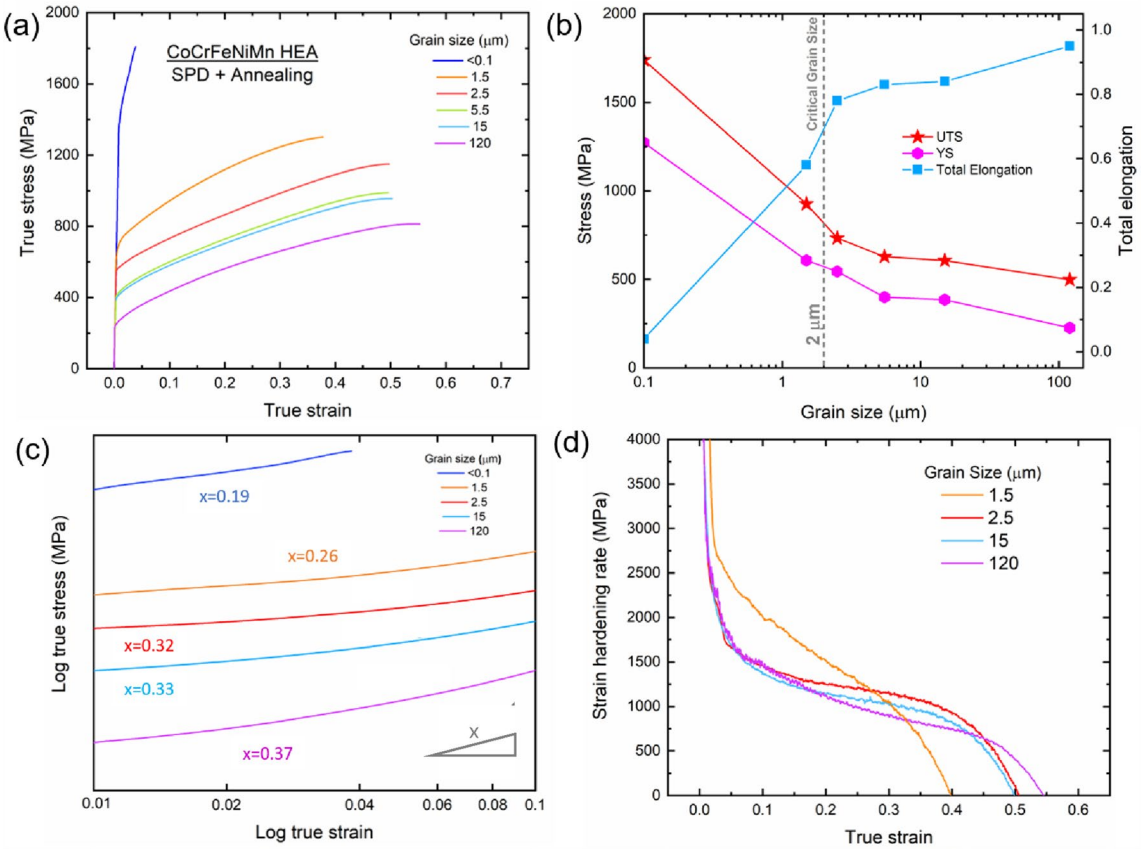

Fig. 4 **a** True stress-true strain plot, **b** Plot of YS, UTS, and total elongation versus grain size, **c** Log true stress versus log true strain in which slope of each line represents the strain hardening exponent and **d** Strain hardening rate versus true strain for different grain sizes

properties of the CoCrFeNiMn HEA for different grain sizes. The results confirm that, with increasing grain size, the yield stress and the tensile strength decrease and the total elongation increases. The results show also that when the grain size reaches ~ 0.1 μm from ~ 120 μm the values of the tensile strength, yield stress and total elongation extend from ~ 1740 MPa, ~ 1270 MPa and ~ 0.04 to ~ 498 MPa, ~ 227 MPa and ~ 0.95, respectively. These values demonstrate that the total elongation decreases significantly at the critical grain size of ~ 2 μm (see Fig. 4b) where this is probably due to a change in the deformation mechanism. The flow curve in the region of uniform deformation is expressed by a power-law relation in which the exponent is known as the strain-hardening exponent. Representative plots of log true stress against log true strain are shown in Fig. 4c where the slopes of the curves give the strain hardening exponents. Thus, the small value of the strain hardening exponent at grain sizes less than ~ 0.1 μm indicates that the sample has very little uniform elongation. The results show this value increases by increasing the grain size. Furthermore, close inspection of these data demonstrates a significant change in the the strain hardening exponent by changing the grain size only from ~ 1.5 to ~ 2.5 μm in the annealed samples. This value then increases slightly after changing the grain size from ultrafine-grains to coarse grain samples of ~ 120 μm.

It is well-established that there is a correlation between the strain hardening exponent value and the deformation mechanism. Figure 4d represents the strain rate hardening against the true strain in which the strain rate hardening curves can be subdivided into three stages depending on the slope variation where there is a rapid decrease of strain rate hardening below a true strain of ~ 0.05 in Stage I, a plateau between a true strain of ~ 0.05 and ~ 0.45 in Stage II and a decrease above a true strain of ~ 0.45 in Stage III. All curves reveal similar behavior except for the curve representing the mechanical behavior of the sample with a grain size of ~ 1.5 μm in which the strain rate hardening curve shows a sharp decrease that is qualitatively similar to Stage I followed by a gradual decrease similar to Stage III that is not representative of the Stage II plateau.

Figure 5 shows ECCI images illustrating the microstructures of fine grain specimens after tensile testing including the presence of annealing and deformation twins as marked

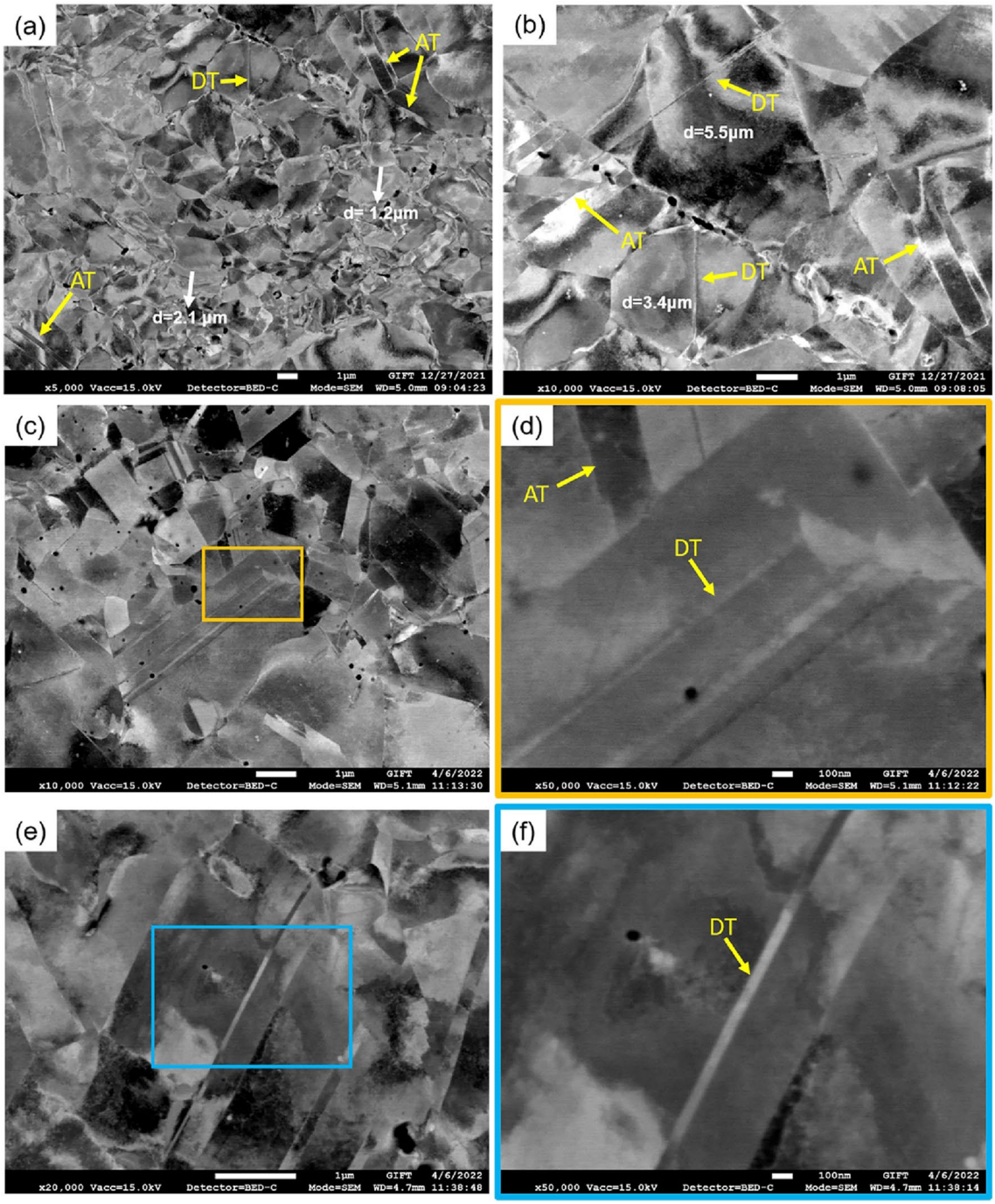

Fig. 5 **a**–**f** Set of ECCI images of fine-grained CoCrFeNiMn HEA samples (after post-deformation annealing) after tensile testing in different magnifications. Higher magnification of areas marked in **c** and **e** are presented in **d** and **f**, respectively. Annealing and deformation twins as marked by AT and DT, respectively

by AT and DT, respectively. These images show that the thickness of the DTs is less than the ATs and these values are in the nanoscale. Close inspection of the microstructures indicates the formation of deformation twins in grains having sizes above ~ 2 μm. Conversely, no deformation twins were detected in grains smaller than ~ 2 μm. The results

clearly suggest the existence of a critical grain size for the formation of deformation twinning which affects the deformation mechanism.

Discussion

Significance of Grain Growth Resistance in Strengthening

The present results confirm the high recrystallization temperature (~ 700 °C) and the high grain growth resistance in this HEA. The high lattice distortion energy and sluggish diffusion, as well as the low SFE in the CoCrFeNiMn HEA, are responsible for this behavior [45–48]. In addition, the results confirm the significance of Cr-rich precipitates in postponing the coarsening by a Zener pinning mechanism in the nano and ultrafine-grained CoCrFeNiMn HEA which is consistent with earlier investigations [24, 49].

Table 1 shows the key parameters representing the grain growth phenomenon in some conventional alloys and the CoCrFeNiMn HEA processed by different procedures. These data reveal that the activation energy, the Q value, of the CoCrFENiMn HEA is very high compared to other conventional alloys. This suggests that the slow grain growth kinetics in HEAs is due to the sluggish diffusion and high lattice distortion. It is important to note also that the Q value for 316L stainless steel is very remarkable as a medium entropy alloy in which molybdenum significantly retards the grain growth towards higher temperatures and slower kinetics and effectively increases the grain growth activation energy due to the interaction energy between Mo and the grain boundaries [44]. Additionally, Table 1 summarizes the information extracted from the grain growth kinetics in the CoCrFeNiMn alloy under different processes. The values of n and the grain growth activation energy for the ball-milled sample are greater than for the other processes. This suggests that grain growth is faster in these conditions than in other conditions which may be due to the high energy that is stored in the ball milling process. The n value reported in this investigation is relatively low compared with the values reported earlier after rolling and milling followed by annealing of similar alloys. This is due to the lower temperature range selected for the post-deformation annealing

Table 1 Summary of key parameters representing grain growth phenomenon in some conventional alloys and CoCrFeNiMn HEA processed by different procedures

Alloy	Condition	Temperature (°C)	n	Q (kJ mol^{-1})	Refs.
Ti–6Al–4V	–	1000–1260	8.9–3.9	227	[50]
2024 (Al)	–	250–350	8.62–8.26	157	[51]
AZ31 (Mg)	–	260–450	5	115	[52]
304 SS	–	850–1050	6.54–2.16	280	[44]
316L SS	–	850–1050	21.74–3.06	568	[44]
Low alloy TRIP steel	–	1150	2	270	[53]
CoCrFeNiMn	HPT	800–950	1.5–2.5	440	This work
CoCrFeNiMn	Cold rolled	850–925	3	322	[54]
CoCrFeNiMn	Ball-milled	800–1100	3.1	197	[55]

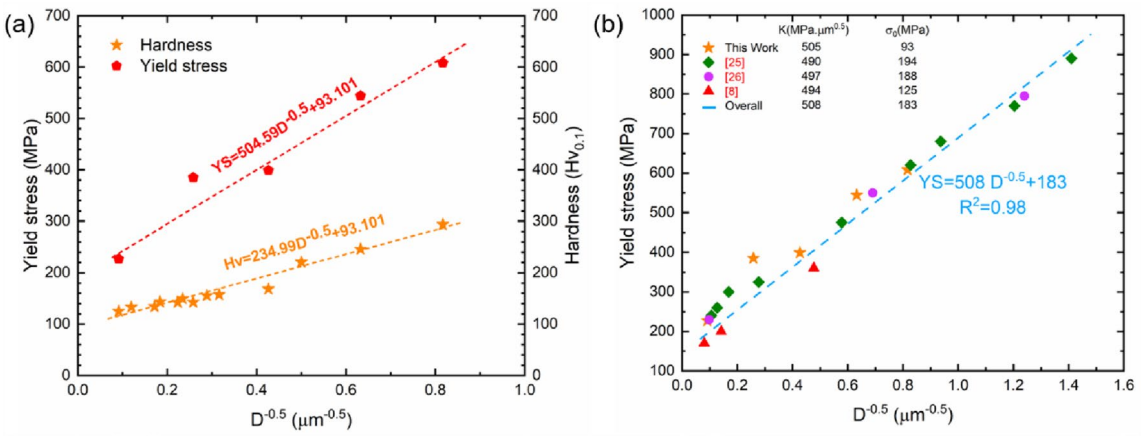

Fig. 6 **a** Yield stress and hardness as a function of grain size in single-phase CoCrFENiMn HEA alloy, and **b** Yield stress as a function of grain size (Hall–Petch plot) to develop a general Hall–Petch relationship for the CoCrFeNiMn HEA alloy [8, 25, 26]

in which decreasing the temperature leads to a slower grain growth and lower n value.

It is well-known that an enhancement of the strength of the alloy can be obtained by grain refinement due to the introduction of a high-volume fraction of grain boundaries that retard the movement of dislocations [56]. The Hall–Petch equation describes the grain boundary strengthening as given by

$$\sigma_{ys} = kD^{-0.5} + \sigma_0 \quad (6)$$

where k, D, and σ_0 are the Hall–Petch strengthening coefficient, the average grain size, and the friction stress, respectively. Figure 6a represents the grain size dependency of the hardness in the form of Hall–Petch plots [57, 58] where the data can be fairly represented by a linear relationship of the form of $Hv \approx 235D^{-0.5} + 93$, where Hv and D are expressed in $Hv_{0.1}$ and μm, respectively. Additionally, the yield stress diagram is also shown in the form of the Hall–Petch relationship in Fig. 6a.

There are several reports on grain boundary strengthening in the CoCrFeNiMn HEA. Nevertheless, they all develop different relationships in a different range of grain sizes. Figure 6b shows the Hall–Petch plot for the CoCrFeNiMn HEA in this study and various other studies [8, 25, 26] in which a general Hall–Petch relationship of $YS = 508D^{-0.5} + 183$ is developed for CoCrFeNiMn HEA in a wide range of grain sizes from ultrafine (< 1 μm) to coarse-grained (> 100 μm). It is important to note that the Hall–Petch strengthening coefficient of the CoCrFeNiMn HEA (~ 508 MPa $\mu m^{0.5}$) is less than conventional materials such as 304L and 316L stainless steels (558 and 546 MPa $\mu m^{0.5}$, respectively) where these are representative low and medium entropy alloys, respectively [59].

Effect of Grain Refinement on the Deformation Mechanism

The deformation mechanism is one of the most important features affecting the ductility of these alloys. The intrinsic characteristics of the material such as the crystal structure, the stacking fault energy and the grain size, together with the deformation temperature, the magnitude of the applied strain and the strain rate during plastic deformation, effectively determine the deformation mechanism in metals and alloys. Thus, it is well-established that dislocation slip, deformation-induced twinning and a deformation-induced martensitic phase transformation are three deformation mechanisms in *fcc* materials that are mainly based on the SFE and the deformation temperature [9]. Deformation-induced twinning is a major deformation mechanism in *fcc* metals when the SFE is lower than ~ 25 mJ m^{-2} [12]. In addition, decreasing the deformation temperature promotes the appearance of other plastic deformation mechanisms along with dislocation slip. Basically, deformation-induced twinning is a well-known deformation mechanism for improving uniform plastic deformation in alloys [10, 60] and the importance of this mechanism in HEAs (such as TWIP HEA) was considered very recently [12, 18].

Previous studies in HEAs and copper alloys also confirm the presence of mechanical twinning [31, 34, 35, 61]. Thus, the results of the present investigation, including the mechanical properties and microstructure investigations, suggest that deformation-induced twinning is an important deformation mechanism that improves the mechanical properties, particularly improving the uniform elongation, but it is fully suppressed in the CoCrFeNiMn HEA when the grain size is less than 2 μm. The reason behind the transition of the deformation mechanism from deformation-induced twinning to dislocation slip is probably the increase in twinning stress with grain refinement [10]. It was shown earlier that the SFE increases by grain refinement when the stacking faults have widths that are narrower than an equilibrium width in fine grains [62]. Accordingly, grain refinement is responsible for suppressing the deformation mechanisms such as deformation-induced twinning and the deformation-induced martensitic phase transformation.

The strain rate hardening plot (Fig. 4d) is a useful way to evaluate the deformation mechanism. As already noted, different behavior was detected in the CoCrFeNiMn in this investigation by decreasing the grain size below a critical value. The strain rate hardening behavior of the samples at Stage I (rapid decrease) can be attributed to the elastic–plastic transition [63, 64] and the strain rate hardening behavior of Stage III, which includes a gradual decrease, indicates a deformation mechanism due to dislocation slip [61, 65]. The strain rate hardening behavior of Stage II, which includes the plateau, indicates a deformation mechanism due to mechanical twinning.

It is important to note that a lower grain size is obtained after high straining by HPT followed by post-deformation annealing at lower temperatures. The strain hardening rate is high when the average grain size is higher due to the easier movement and generation of dislocations and also the formation of deformation twins which provides higher elongation during deformation. Basically, deformation twinning increases strain hardening and therefore increases the uniform deformation in which a lack of twinning formation during plastic deformation in very small grain size (< 2 μm) materials leads to a lower strain hardening.

Based on the results from this investigation, Fig. 7 schematically illustrates the deformation mechanism in different grain sizes for the CoCrFeNiMn HEA. The results show that the deformation mechanism at grain sizes below ~ 2 μm is based only on dislocation slip whereas at grain sizes larger

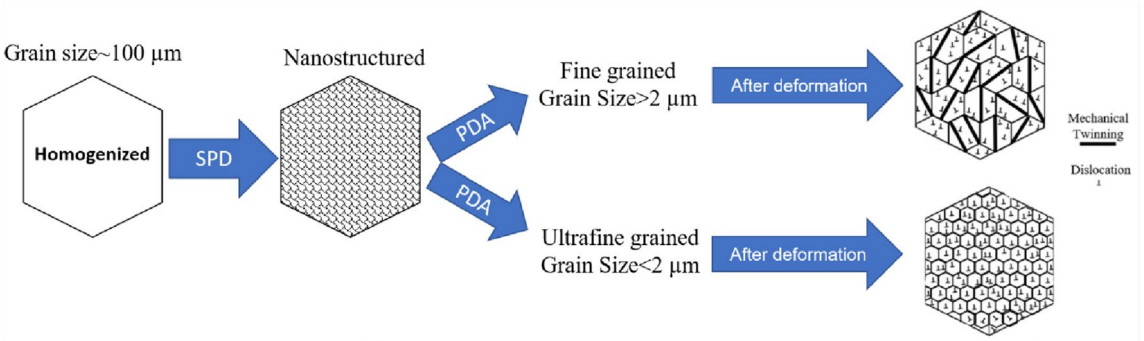

Fig. 7 Schematic diagram showing the microstructural evolution in CoCrFeNiMn HEA having different grain sizes during plastic deformation

than ~ 2 μm deformation-induced twinning is also effective in addition to dislocation slip.

A Model to Optimize the Grain Size

The present results show clearly that deformation-induced twinning is suppressed at grain sizes less than a critical size of ~ 2 μm. It is important to note that twinning is responsible for the high ductility at low temperatures by providing an additional deformation mode [8]. In addition, the deformation-induced twinning is responsible for significant grain refinement after imposing sufficient strain during plastic deformation by the dynamic Hall–Petch effect which decreases the dislocation mean free path and thereby increases the strength of the material [18]. Accordingly, controlling the grain size by conducting an effective thermomechanical treatment, including plastic deformation followed by annealing, is important in order to tailor a fine-grained microstructure and improve the strength by activating deformation-induced twinning without any significant sacrifice of ductility. In the following, a model is derived to control the grain size immediately above the critical grain size of ~ 2 μm in the fine-grain range to benefit from the advantages of deformation-induced twining in the CoCrFeNiMn HEA.

According to Eqs. 3 and 5, the time and temperature of annealing can be obtained by imposing D_{critical}, k_0, Q, and R in Eq. 7 to derive Eq. 8:

$$\text{Ln}t = n\text{Ln}D_{\text{critical}} - \left(\text{Ln}k_0 - \frac{Q}{RT}\right) \tag{7}$$

and

$$\text{Ln}t = n\text{Ln}2 - \left(48 - \frac{53387}{T}\right) \tag{8}$$

Figure 8a shows the grain growth exponent value, n, represented in Fig. 3b against the temperature (K) which gives a linear relationship in the form of $n = 0.0056\ T - 4.52$, where T is expressed in K. Accordingly, Eq. 9 can be derived by putting the n value in Eq. 7 so that

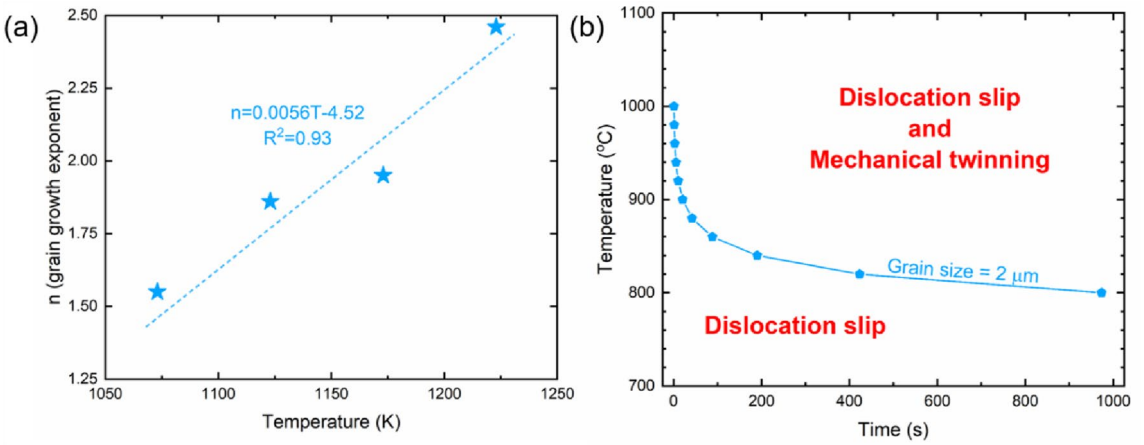

Fig. 8 **a** Grain growth exponent, n, against temperature. **b** Temperature against the time of annealing in order to deduce the optimum grain size

$$\begin{aligned} \mathrm{Ln}t &= (0.0056T - 4.52)\mathrm{Ln}2 - \left(48 - \frac{53387}{T}\right) \\ &= 0.0039T + \frac{53387}{T} - 44.9 \end{aligned} \tag{9}$$

The above equation represents a guiding curve, as illustrated in Fig. 8b, for controlling the grain size with optimum mechanical properties. These data show that the temperature and time of post-deformation annealing must be in the upper region in order to activate the deformation-induced twinning in grains. Therefore, it can be considered as a model to tailor the microstructure by an appropriate thermomechanical treatment to achieve a good combination of strength and ductility in different HEAs.

Summary and Conclusions

1. Grain growth behavior was studied systematically during the annealing of a severely deformed CoCrFeNiMn HEA. The results revealed significant coarsening at temperatures > 800 °C due to the dissolution of precipitates together with a high rate of diffusion at high temperatures. The microstructure showed a wide range of grain sizes from ~ 0.05 to ~ 70 μm after SPD and after annealing at 1000 °C, respectively.
2. The results show that the value of the grain growth exponent, n, increased with increasing annealing temperature. In addition, the value of the grain growth activation energy, Q, is equal to ~ 440 kJ mol^{-1} which is a significant value by comparison with other conventional alloys. The results suggest a general Hall–Petch relationship of the form $YS = 508D^{-0.5} + 183$ for the CoCrFeNiMn HEA over a wide range of grain sizes from the ultrafine (< 1 μm) to coarse grained (> 100 μm).
3. The results suggest that there is a critical grain size of ~ 2 μm at which the total elongation decreases significantly due to a suppression of the activation of deformation-induced twinning as a useful deformation mechanism together with slip to improve the mechanical properties. A model is proposed to determine the optimum grain size by controlling the temperature and time of annealing in the range of fine grain sizes in order to benefit from the advantages of deformation-induced twining in the CoCrFeNiMn HEA.

Author Contributions HS: Conceptualization, Methodology, Formal analysis, Visualization, Writing—original draft. MSM: Methodology, Data curation, Writing—original draft. SAS: Investigation, Formal analysis, Writing—review & editing. CSL: Supervision, Resources, Writing—review & editing. TGL: Supervision, Resources, Project administration, Writing—review & editing.

Funding One of the authors was supported by the European Research Council under ERC Grant Agreement No. 267464-SPDMETALS (TGL). There was no other financial support.

Data Availability The raw/processed data required to reproduce these findings cannot be shared at this time as the data also forms part of an ongoing study.

Code Availability Not applicable.

Declarations

Competing Interests The authors declare that they have no known competing financial interests or personal relationships that could have appeared of influence the work reported in this paper.

References

1. B. Cantor, I. Chang, P. Knight, A. Vincent, Microstructural development in equiatomic multicomponent alloys. Mater. Sci. Eng. A **375**, 213–218 (2004)
2. J.W. Yeh, S.K. Chen, S.J. Lin, J.Y. Gan, T.S. Chin, T.T. Shun, C.H. Tsau, S.Y. Chang, Nanostructured high-entropy alloys with multiple principal elements: novel alloy design concepts and outcomes. Adv. Eng. Mater. **6**(5), 299–303 (2004)
3. Y. Tian, S. Sun, H. Lin, Z. Zhang, Fatigue behavior of CoCrFeMnNi high-entropy alloy under fully reversed cyclic deformation. J. Mater. Sci. Technol. **35**(3), 334–340 (2019)
4. Y.J. Kwon, J.W. Won, S.H. Park, J.H. Lee, K.R. Lim, Y.S. Na, C.S. Lee, Ultrahigh-strength CoCrFeMnNi high-entropy alloy wire rod with excellent resistance to hydrogen embrittlement. Mater. Sci. Eng. A **732**, 105–111 (2018)
5. F. Otto, A. Dlouhý, K.G. Pradeep, M. Kuběnová, D. Raabe, G. Eggeler, E.P. George, Decomposition of the single-phase high-entropy alloy CrMnFeCoNi after prolonged anneals at intermediate temperatures. Acta Mater. **112**, 40–52 (2016)
6. M.S. Mehranpour, H. Shahmir, M. Nili-Ahmadabadi, Microstructure and excess free volume of severely cold shape rolled CoCrFeNiMn high entropy alloy. J. Alloys Compd. **840**, 155672 (2020)
7. H. Shahmir, J. He, Z. Lu, M. Kawasaki, T.G. Langdon, Effect of annealing on mechanical properties of a nanocrystalline CoCrFeNiMn high-entropy alloy processed by high-pressure torsion. Mater. Sci. Eng. A **676**, 294–303 (2016)
8. F. Otto, A. Dlouhý, C. Somsen, H. Bei, G. Eggeler, E.P. George, The influences of temperature and microstructure on the tensile properties of a CoCrFeMnNi high-entropy alloy. Acta Mater. **61**(15), 5743–5755 (2013)
9. H. Shahmir, P. Asghari-Rad, M.S. Mehranpour, F. Forghani, H.S. Kim, M. Nili-Ahmadabadi, Evidence of FCC to HCP and BCC-martensitic transformations in a CoCrFeNiMn high-entropy alloy by severe plastic deformation. Mater. Sci. Eng. A **807**, 140875 (2021)
10. S. Sun, Y. Tian, H. Lin, H. Yang, X. Dong, Y. Wang, Z. Zhang, Transition of twinning behavior in CoCrFeMnNi high entropy alloy with grain refinement. Mater. Sci. Eng. A **712**, 603–607 (2018)

11. A. Zaddach, C. Niu, C. Koch, D. Irving, Mechanical properties and stacking fault energies of NiFeCrCoMn high-entropy alloy. JOM **65**(12), 1780–1789 (2013)
12. M.S. Mehranpour, H. Shahmir, P. Asghari-Rad, M. Hosseinzadeh, N. Rasooli, H.S. Kim, M. Nili-Ahmadabadi, Upgrading of superior strength–ductility trade-off of CoCrFeNiMn high-entropy alloy by microstructural engineering. Materialia **22**, 101394 (2022)
13. N. Stepanov, M. Tikhonovsky, N. Yurchenko, D. Zyabkin, M. Klimova, S. Zherebtsov, A. Efimov, G. Salishchev, Effect of cryodeformation on structure and properties of CoCrFeNiMn high-entropy alloy. Intermetallics **59**, 8–17 (2015)
14. S. Liu, Y. Wu, H. Wang, J. He, J. Liu, C. Chen, X. Liu, H. Wang, Z. Lu, Stacking fault energy of face-centered-cubic high entropy alloys. Intermetallics **93**, 269–273 (2018)
15. J.-E. Ahn, Y.-K. Kim, S.-H. Yoon, K.-A. Lee, Tuning the microstructure and mechanical properties of cold sprayed equiatomic CoCrFeMnNi high-entropy alloy coating layer. Met. Mater. Int. **27**, 6–15 (2020)
16. Y. Kim, H.K. Park, P. Asghari-Rad, J. Jung, J. Moon, H.S. Kim, Constitutive modeling with critical twinning stress in CoCrFeMnNi high entropy alloy at cryogenic temperature and room temperature. Met. Mater. Int. **27**, 2300–2309 (2020)
17. D. Wei, X. Li, S. Schönecker, J. Jiang, W.-M. Choi, B.-J. Lee, H.S. Kim, A. Chiba, H. Kato, Development of strong and ductile metastable face-centered cubic single-phase high-entropy alloys. Acta Mater. **181**, 318–330 (2019)
18. J. Moon, O. Bouaziz, H.S. Kim, Y. Estrin, Twinning engineering of a CoCrFeMnNi high-entropy alloy. Scr. Mater. **197**, 113808 (2021)
19. J.W. Won, S. Lee, S.H. Park, M. Kang, K.R. Lim, C.H. Park, Y.S. Na, Ultrafine-grained CoCrFeMnNi high-entropy alloy produced by cryogenic multi-pass caliber rolling. J. Alloys Compd. **742**, 290–295 (2018)
20. X. Ma, J. Chen, X. Wang, Y. Xu, Y. Xue, Microstructure and mechanical properties of cold drawing CoCrFeMnNi high entropy alloy. J. Alloys Compd. **795**, 45–53 (2019)
21. B. Schuh, F. Mendez-Martin, B. Völker, E.P. George, H. Clemens, R. Pippan, A. Hohenwarter, Mechanical properties, microstructure and thermal stability of a nanocrystalline CoCrFeMnNi high-entropy alloy after severe plastic deformation. Acta Mater. **96**, 258–268 (2015)
22. S. Sun, Y. Tian, H. Lin, H. Yang, X. Dong, Y. Wang, Z. Zhang, Achieving high ductility in the 1.7 GPa grade CoCrFeMnNi high-entropy alloy at 77 K. Mater. Sci. Eng. A **740**, 336–341 (2019)
23. J. Gu, M. Song, Annealing-induced abnormal hardening in a cold rolled CrMnFeCoNi high entropy alloy. Scr. Mater. **162**, 345–349 (2019)
24. M.S. Mehranpour, H. Shahmir, A. Derakhshandeh, M. Nili-Ahmadabadi, Significance of Ti addition on precipitation in CoCrFeNiMn high-entropy alloy. J. Alloys Compd. **888**, 161530 (2021)
25. S. Sun, Y. Tian, H. Lin, X. Dong, Y. Wang, Z. Zhang, Z. Zhang, Enhanced strength and ductility of bulk CoCrFeMnNi high entropy alloy having fully recrystallized ultrafine-grained structure. Mater. Des. **133**, 122–127 (2017)
26. S. Sun, Y. Tian, H. Lin, X. Dong, Y. Wang, Z. Wang, Z. Zhang, Temperature dependence of the Hall–Petch relationship in CoCrFeMnNi high-entropy alloy. J. Alloys Compd. **806**, 992–998 (2019)
27. J. Gu, S. Ni, Y. Liu, M. Song, Regulating the strength and ductility of a cold rolled FeCrCoMnNi high-entropy alloy via annealing treatment. Mater. Sci. Eng. A **755**, 289–294 (2019)
28. Z. Li, L. Fu, H. Zheng, R. Yu, L. Lv, Y. Sun, X. Dong, A. Shan, Effect of annealing temperature on microstructure and mechanical properties of a severe cold-rolled FeCoCrNiMn high-entropy alloy. Metall. Mater. Trans. A **50**(7), 3223–3237 (2019)
29. M. Klimova, D. Shaysultanov, S. Zherebtsov, N. Stepanov, Effect of second phase particles on mechanical properties and grain growth in a CoCrFeMnNi high entropy alloy. Mater. Sci. Eng. A **748**, 228–235 (2019)
30. B. Gludovatz, A. Hohenwarter, D. Catoor, E.H. Chang, E.P. George, R.O. Ritchie, A fracture-resistant high-entropy alloy for cryogenic applications. Science **345**(6201), 1153–1158 (2014)
31. G. Laplanche, A. Kostka, O. Horst, G. Eggeler, E. George, Microstructure evolution and critical stress for twinning in the CrMnFeCoNi high-entropy alloy. Acta Mater. **118**, 152–163 (2016)
32. S.-H. Joo, H. Kato, M. Jang, J. Moon, C. Tsai, J. Yeh, H. Kim, Tensile deformation behavior and deformation twinning of an equimolar CoCrFeMnNi high-entropy alloy. Mater. Sci. Eng. A **689**, 122–133 (2017)
33. J.-Y. Lee, J.-S. Hong, S.-H. Kang, Y.-K. Lee, The effect of austenite grain size on deformation mechanism of Fe–17Mn steel. Mater. Sci. Eng. A **809**, 140972 (2021)
34. P. Asghari-Rad, P. Sathiyamoorthi, J.W. Bae, J. Moon, J.M. Park, A. Zargaran, H.S. Kim, Effect of grain size on the tensile behavior of $V_{10}Cr_{15}Mn_5Fe_{35}Co_{10}Ni_{25}$ high entropy alloy. Mater. Sci. Eng. A **744**, 610–617 (2019)
35. Y. Tian, L. Zhao, S. Chen, A. Shibata, Z. Zhang, N. Tsuji, Significant contribution of stacking faults to the strain hardening behavior of Cu-15% Al alloy with different grain sizes. Sci. Rep. **5**(1), 1–9 (2015)
36. A.P. Zhilyaev, T.G. Langdon, Using high-pressure torsion for metal processing: fundamentals and applications. Prog. Mater Sci. **53**(6), 893–979 (2008)
37. R.B. Figueiredo, P.R. Cetlin, T.G. Langdon, Using finite element modeling to examine the flow processes in quasi-constrained high-pressure torsion. Mater. Sci. Eng. A **528**(28), 8198–8204 (2011)
38. M.S. Mehranpour, H. Shahmir, M. Nili-Ahmadabadi, CoCrFeNiMn high entropy alloy microstructure and mechanical properties after severe cold shape rolling and annealing. Mater. Sci. Eng. A **793**, 139884 (2020)
39. M.S. Mehranpour, H. Shahmir, M. Nili-Ahmadabadi, Precipitation kinetics in heavily deformed CoCrFeNiMn high entropy alloy. Mater. Lett. **288**, 129359 (2021)
40. N. Stepanov, D. Shaysultanov, M. Ozerov, S. Zherebtsov, G. Salishchev, Second phase formation in the CoCrFeNiMn high entropy alloy after recrystallization annealing. Mater. Lett. **185**, 1–4 (2016)
41. H. Shahmir, T. Mousavi, J. He, Z. Lu, M. Kawasaki, T.G. Langdon, Microstructure and properties of a CoCrFeNiMn high-entropy alloy processed by equal-channel angular pressing. Mater. Sci. Eng. A **705**, 411–419 (2017)
42. F. Najafkhani, S. Kheiri, B. Pourbahari, H. Mirzadeh, Recent advances in the kinetics of normal/abnormal grain growth: a review. Arch. Civ. Mech. Eng. **21**(1), 1–20 (2021)
43. X.-M. Chen, Y. Lin, F. Wu, EBSD study of grain growth behavior and annealing twin evolution after full recrystallization in a nickel-based superalloy. J. Alloys Compd. **724**, 198–207 (2017)
44. M. Naghizadeh, H. Mirzadeh, Elucidating the effect of alloying elements on the behavior of austenitic stainless steels at elevated temperatures. Metall. Mater. Trans. A **47**(12), 5698–5703 (2016)
45. P. Bhattacharjee, G. Sathiaraj, M. Zaid, J. Gatti, C. Lee, C.-W. Tsai, J.-W. Yeh, Microstructure and texture evolution during annealing of equiatomic CoCrFeMnNi high-entropy alloy. J. Alloys Compd. **587**, 544–552 (2014)
46. G. Sathiaraj, C. Tsai, J. Yeh, M. Jahazi, P.P. Bhattacharjee, The effect of heating rate on microstructure and texture formation during annealing of heavily cold-rolled equiatomic CoCrFeMnNi high entropy alloy. J. Alloys Compd. **688**, 752–761 (2016)

47. G.D. Sathiaraj, P.P. Bhattacharjee, Effect of cold-rolling strain on the evolution of annealing texture of equiatomic CoCrFeMnNi high entropy alloy. Mater. Charact. **109**, 189–197 (2015)
48. G.D. Sathiaraj, P.P. Bhattacharjee, C.-W. Tsai, J.-W. Yeh, Effect of heavy cryo-rolling on the evolution of microstructure and texture during annealing of equiatomic CoCrFeMnNi high entropy alloy. Intermetallics **69**, 1–9 (2016)
49. H. Shahmir, M.S. Mehranpour, A. Derakhshandeh, M. Nili-Ahmadabadi, Microstructure tailoring to enhance mechanical properties in CoCrFeNiMn high-entropy alloy by Ti addition and thermomechanical treatment. Mater. Charact. **182**, 111513 (2021)
50. O. Ivasishin, S. Shevchenko, S. Semiatin, Effect of crystallographic texture on the isothermal beta grain-growth kinetics of Ti–6Al–4V. Mater. Sci. Eng. A **332**(1–2), 343–350 (2002)
51. Z. Huda, T. Zaharinie, Kinetics of grain growth in 2024-T3: an aerospace aluminum alloy. J. Alloys Compd. **478**(1–2), 128–132 (2009)
52. J.J. Bhattacharyya, S. Agnew, G. Muralidharan, Texture enhancement during grain growth of magnesium alloy AZ31B. Acta Mater. **86**, 80–94 (2015)
53. G. Azizi, H. Mirzadeh, M. HabibiParsa, Unraveling the effect of homogenization treatment on decomposition of austenite and mechanical properties of low-alloyed TRIP steel. Steel Res. Int. **87**(7), 820–823 (2016)
54. W. Liu, Y. Wu, J. He, T. Nieh, Z. Lu, Grain growth and the Hall–Petch relationship in a high-entropy FeCrNiCoMn alloy. Scr. Mater. **68**(7), 526–529 (2013)
55. M. Vaidya, A. Anupam, J.V. Bharadwaj, C. Srivastava, B. Murty, Grain growth kinetics in CoCrFeNi and CoCrFeMnNi high entropy alloys processed by spark plasma sintering. J. Alloys Compd. **791**, 1114–1121 (2019)
56. E. Hall, The deformation and ageing of mild steel: III discussion of results. Proc. Phys. Soc. Lond. Sect. B **64**(9), 747 (1951)
57. H. Yu, Y. Xin, M. Wang, Q. Liu, Hall–Petch relationship in Mg alloys: a review. J. Mater. Sci. Technol. **34**(2), 248–256 (2018)
58. M.S. Mehranpour, A. Heydarinia, M. Emamy, H. Mirzadeh, A. Koushki, R. Razi, Enhanced mechanical properties of AZ91 magnesium alloy by inoculation and hot deformation. Mater. Sci. Eng. A **802**, 140667 (2020)
59. M.J. Sohrabi, H. Mirzadeh, C. Dehghanian, Significance of martensite reversion and austenite stability to the mechanical properties and transformation-induced plasticity effect of austenitic stainless steels. J. Mater. Eng. Perform. **29**, 3233–3234 (2020)
60. J. Moon, O. Bouaziz, H.S. Kim, Y. Estrin, Twinning engineering of high-entropy alloys: an exercise in process optimization and modeling. Mater. Sci. Eng. A **822**, 141681 (2021)
61. E. El-Danaf, S.R. Kalidindi, R.D. Doherty, Influence of grain size and stacking-fault energy on deformation twinning in fcc metals. Metall. Mater. Trans. A **30**(5), 1223–1233 (1999)
62. S.Y. Jo, J. Han, J.-H. Kang, S. Kang, S. Lee, Y.-K. Lee, Relationship between grain size and ductile-to-brittle transition at room temperature in Fe–18Mn–0.6 C–15 Si twinning-induced plasticity steel. J. Alloys Compd. **627**, 374–382 (2015)
63. M.J. Jang, D.-H. Ahn, J. Moon, J.W. Bae, D. Yim, J.-W. Yeh, Y. Estrin, H.S. Kim, Constitutive modeling of deformation behavior of high-entropy alloys with face-centered cubic crystal structure. Mater. Res. Lett. **5**(5), 350–356 (2017)
64. J.M. Park, J. Moon, J.W. Bae, M.J. Jang, J. Park, S. Lee, H.S. Kim, Strain rate effects of dynamic compressive deformation on mechanical properties and microstructure of CoCrFeMnNi high-entropy alloy. Mater. Sci. Eng. A **719**, 155–163 (2018)
65. S. Asgari, E. El-Danaf, S.R. Kalidindi, R.D. Doherty, Strain hardening regimes and microstructural evolution during large strain compression of low stacking fault energy fcc alloys that form deformation twins. Metall. Mater. Trans. A **28**(9), 1781–1795 (1997)